Chapter 6
Interface Strength Assessments of Sandwich Panels with a Face Sheet/Core Debond

Vyacheslav N. Burlayenko, Holm Altenbach, and Svetlana D. Dimitrova

Abstract Virtual fracture tests combining analytical considerations and a finite element analysis are performed to provide assessment of face sheet-to-core interface strength in sandwich panels. Three fracture test methods, different in laboratory testing procedures and virtual modeling solutions, such as sandwich double cantilever beam subjected to uneven bending moments (DCB-UBM), sandwich double cantilever beam (DCB) and sandwich single cantilever beam (SCB) specimens are examined with the aim to predict the fracture parameters - energy-release rate (ERR) and stress-intensity factors (SIFs) - required for the assessment of the interface strength within the framework of linear elastic fracture mechanics (LEFM). The existence of mode mixity at the bi-material interface of a sandwich panel is considered and appropriate methods applied for mode decomposition are described. The numerical analyses are carried out using the capabilities of the ABAQUS code. In general, good agreement between the results of numerically calculated fracture parameters and those obtained using analytical solutions and/or from experimental data available in the literature is observed. Finally, computational aspects of the numerical models have been revisited and put into perspective of the accurate and efficient interface strength assessments of sandwich panels.

Vyacheslav N. Burlayenko
Department of Applied Mathematics, National Technical University KhPI, 2 Kyrpychova str., 61002 Kharkiv, Ukraine
e-mail: burlayenko@yahoo.com

Holm Altenbach
Institut für Mechanik, Otto-von-Guericke-Universität Magdeburg, Universitätsplatz 2, 39106 Magdeburg, Germany
e-mail: holm.altenbach@ovgu.de

Svetlana D. Dimitrova
Department of Higher Mathematics, National Technical University KhPI, 2 Kyrpychova str., 61002 Kharkiv, Ukraine
e-mail: s.dimitrovaburlayenko@gmail.com

H. Altenbach et al. (eds.), *Analysis of Shells, Plates, and Beams*, Advanced Structured Materials 134,
https://doi.org/10.1007/978-3-030-47491-1_6

Key words: Sandwich panels · Face sheet/core interface strength · Fracture test methods · Finite element analysis

6.1 Introduction

A sandwich panel consists of three material layers such as a low-density core and two thin stiff face sheets bonded to each side of the core (Altenbach et al, 2018). Due to this design, sandwich panels have been widely used in various engineering applications, for which an efficient combination of high structural rigidity and low weight is required and/or whose structural properties should meet particular design features (Harne et al, 2012; Xie et al, 2016; Mouritz, 2017; Chatterjee et al, 2019). The layered structure of sandwich panels makes a premise to their inevitable susceptibility to interfacial damage between the constitutive material layers, the so-called face sheet-to-core debonding. Theoretical and experimental studies have already shown that this defect decreases the overall load-bearing capacity of sandwich panels and gives rise to quantitative and qualitative changes of their dynamic responses (Burlayenko and Sadowski, 2011a; Idriss and Mahi, 2017; Pölöskei and Szekrényes, 2017; Qu and Meng, 2017; Burlayenko and Sadowski, 2018). The latter features are exploited for identifying and quantifying such type of damage within sandwich panes as discussed, e.g., in Burlayenko and Sadowski (2011b); Mustapha and Ye (2013); Farhana et al (2016); Lu et al (2017); Seguel and Meruane (2018). The relevance of such structural monitoring techniques is justified by the evidence that the debonding propagation can lead to eventual failure of sandwich structures (Triantafillou and Gibson, 1987; Burlayenko and Sadowski, 2014). Therefore, sandwich panels should be validated in terms of damage tolerance and possible failure.

The structural integrity of the sandwich structure is defined by the strength of its face sheet/core interface. Traditionally, the debonding between the face sheet and the core is treated as an interfacial bi-material crack, and the interface strength is quantified using the concept of interface fracture toughness within the framework of linear elastic fracture mechanics (LEFM) (Willis, 1971). Fracture specimens are used to supply necessary information regarding the interface strength. Hence, by analysing the specimens' behaviour with experimental, analytical or numerical methods, the fracture parameters such as stress-intensity factors (SIFs) or energy-release rates (ERRs) controlling the fracture process at the crack tip are obtained.

A variety of test configurations towards the face sheet/core-strength assessment of sandwich panels have been proposed during the last two decades. Some of the most popular specimens' geometries being studied in an attempt to define interfacial fracture toughness in pure or mixed fracture modes are listed in Shivakumar and Smith (2004). The strength of the face sheet/core bond corresponding to the lowest critical ERR has traditionally been measured using a double cantilever sandwich beam (DCB) (Prasad and Carlsson, 1994; Avilés and Carlsson, 2008). An alternative test method for generation of mode I dominated fracture is a single cantilever sandwich beam (SCB) as proposed in Cantwell and Davies (1996) and further improved

in Ratcliffe and Reeder (2011); Rinker et al (2011); Adams et al (2012). In order to characterize the interfacial shear strength of sandwich panels, a cracked sandwich beam (CSB) specimen developed in Carlsson et al (1991) or its modifications, e.g. Cantwell et al (1999), accommodating the sliding deformation between the face sheet and the core through three-point bending are often used. However, while the studies on the pure (strictly speaking - dominated) modes I and II are important, they are not sufficient for evaluating interface fracture toughness of sandwich panels. Dillard et al (2009) presented the findings for adhesive joints, which are similar to sandwich panels, where the most critical ERR occurs at a certain I/II mode mixity. Moreover, recently it has been recognized that the mode-III deformation and its different combinations (i.e. mixed mode I/III, II/III and even I/II/III) are also essential for the complete fracture characterization of advanced composite materials (Hernández-Pérez et al, 2013). Although some test methods have been proposed for the determination of interfacial fracture toughness involving the tearing mode, all of them have yet unresolved issues which restrain their standardization. The main issues in these test methods relate to difficulties to produce a pure mode III fracture state at the debonding front, difficulties to track the crack propagation, uncertainty in the data reduction methods and/or complexity of the test rig (Rodríguez-González et al, 2014). Thereby, the mode I and II mixity as the simplest case of mixed mode fracture is commonly analyzed in sandwich materials so far. For studying mixed mode I/II fracture, the mixed mode bending (MMB) test devised earlier for laminated composites has been adapted to sandwich structures as done in Quispitupa et al (2009). Other methods for mixed mode I/II testing has been derived from the DCB and SCB test configurations such as a double cantilever sandwich beam subjected to uneven bending moments (DCB-UBM) (Sorensen et al, 2006) and a titled sandwich debonded (TSD) specimen (Li and Carlsson, 1999), respectively.

The majority of analytical solutions relevant to the extraction of ERR or SIFs from the tests mentioned above have been found by reducing the dimension of the problem. Efficient structural models presenting the specimens as an assemblage of beams or plates can be found in Valvo et al (2015); Saseendran et al (2018); Massabò and Campi (2014); Odessa et al (2018); Kiss and Szekrényes (2019), just to name few recent publications. In doing so, either classical or first-or higher order shear-deformation structural theories as well as assumptions on either rigid or flexibile flexible deformability ahead of the crack tip within the intact part are used for analysing the specimen's behaviour. Some aspects of interface fracture analysis in layered structures can be found in Thouless (2018). Moreover, since the face sheet/core interface has a bimaterial nature, the fracture analysis must recognize the mixed mode loading and be able to define the relative amount of mode I and mode II at the debonding tip. A great effort has been made to obtain such mode partition. For this either semi-analytic (numerical) solutions for particular loading cases within the interface LEFM concepts (Suo and Hill, 1990; Li et al, 2004; Kardomateas et al, 2013) or the structural models (Williams, 1988; Bruno and Greco, 2001; Wang and Qiao, 2004; Andrews and Massabò, 2007) for the fracture specimens have been exploited. Herewith, two approaches are used. The first one referred to as local approach considers debonding conditions as local stresses at the crack tip (Suo and

Hutchinson, 1990; Li et al, 2004). Alternatively, the second one is a global approach that evaluates the ERR as the first variation of the total potential energy with respect to the advancing crack area (Williams, 1988).

In an attempt to improve the accuracy of data evaluation in the tests, two- and three-dimensional analytical elasticity solutions have also been applied to the fracture analysis. In Fichter (1983); Georgiadis and Papadopoulos (1990), the exact 2-D elasticity solutions of the DCB have been obtained by using the Wiener-Hopf technique. On the other hand, the 2-D elasticity solutions are limited by the assumption of either plane stress or plane strain conditions. As a result, they are not able to capture an actual curved crack front (thumb nail shaped) associated with Poisson-strain effect under specimen bending (Samborski, 2018). Therefore, 3-D elasticity models are obviously the most accurate, but their solutions can only be obtained by using numerical methods, in particular the finite element method (FEM) (Williams and Addessio, 1997; Davis et al, 2014). Two-dimensional debonding problems have also broadly been reported in the literature by using the FEM. It has been reported if the effect of front curvature is not a main concern, the less sophisticated 2-D models would be sufficiently accurate for performing the fracture analysis (Crews et al, 1991). The FEM provides efficient techniques for the mode partitioning in bimaterial interfacial cracks. These techniques include the displacement or stress interpretation methods (Kuna, 2013), the crack surface displacement method (Smelser, 1979), the interaction integral approach based on the path independent integral technique (Shih and Asaro, 1988), the virtual crack extension (VCE) (Matos et al, 1989) and virtual crack closure techniques (VCCT) (Beuth, 1996). In addition, a large number of studies involving the strength prediction of layered structures including sandwich composites use the crack tip element approach (Davidson et al, 1995).

This paper extends some preliminary considerations by Burlayenko et al (2018, 2019c,b,a) in the light of new findings in the recent literature on interfacial strength assessments of sandwich materials. The study is aimed at understanding and reproducing the features of interfacial cracking, which are observed in the DCB-UBM, DCB and SCB sandwich specimens broadly used for fracture testing. In addition to these experimental aspects, both analytical and numerical calculations are presented to explain how the ERR and SIFs are derived from the frature test data for those specimens. Comparisons between analytical and numerical solutions and experimental data available in the literature are also given. Finally, the accuracy of the theoretical predictions is discussed.

6.2 Mechanics of Bi-material Interface Cracks

A complexity in analysing bi-material interface cracks is that such cracks generally exhibit tension-shear coupling effects even under pure opening or shearing loading. Also, the oscillations of stress and displacement fields, increasing when approaching the crack tip, from the standpoint of LEFM (Hutchinson and Suo, 1991). Thus, to characterise the singular stress and displacement fields, a complex stress-intensity factor

(SIF), K, together with the oscillation index, ϵ, relating to the elastic properties of the materials are utilized (Rice, 1988). Following Suo and Hill (1990); Kuang-Chong (1991) the structure of the asymptotic near-tip fields for an interface crack results from the solution of the eigenvalue problem induced by the traction free boundary conditions on the crack flanks as

$$\bar{\mathbf{H}}\mathbf{w} = e^{2\pi\epsilon}\mathbf{H}\mathbf{w}, \tag{6.1}$$

where $\mathbf{H}$ is a 3×3 positive defined compliance-like Hermitian matrix involving the bi-material elastic constants and $\bar{\mathbf{H}}$ is its complex conjugate matrix. Three eigenpairs such as $(\epsilon,\mathbf{w})$, $(-\epsilon,\bar{\mathbf{w}})$ and $(0,w_3)$, where $\mathbf{w}$, $\bar{\mathbf{w}}$ and w_3 are complex, complex conjugate and real eigenvectors, respectively, are the solutions of (6.1).

In the 2-D case of the interface crack between two dissimilar orthotropic materials, where the material symmetry axes are aligned along the interface (Fig. 6.1b), the matrix $\mathbf{H}$ takes the form (Wang et al, 1992):

$$\begin{aligned} H_{11} &= \left[2n\lambda^{1/4}\sqrt{s_{11}s_{22}}\right]_{\#1} + \left[2n\lambda^{1/4}\sqrt{s_{11}s_{22}}\right]_{\#2}, \\ H_{22} &= \left[2n\lambda^{-1/4}\sqrt{s_{11}s_{22}}\right]_{\#1} + \left[2n\lambda^{-1/4}\sqrt{s_{11}s_{22}}\right]_{\#2}, \\ H_{12} &= \bar{H}_{21} = \left[\sqrt{s_{11}s_{22}}+s_{12}\right]_{\#2} - \left[\sqrt{s_{11}s_{22}}+s_{12}\right]_{\#1}, \end{aligned} \tag{6.2}$$

where s_{ij}, $s_{16}=s_{26}=0$, $i,j=1,2,6$ are components of the compliance matrix of the orthotropic material (#1 or #2) in plane stress; in plane strain the compliances are

$$\tilde{s}_{ij} = s_{ij} - \frac{s_{i3}s_{j3}}{s_{33}}$$

Note that

$$\lambda = \frac{s_{11}}{s_{22}} = \frac{E_2}{E_1}$$

and

$$\varrho = \frac{2s_{12}+s_{66}}{2\sqrt{s_{11}s_{22}}} = \frac{\sqrt{E_1E_2}}{2G_{12}} - \sqrt{\nu_{12}\nu_{21}}$$

are parameters of anisotropy and

$$n = \sqrt{\frac{(1+\varrho)}{2}}.$$

The solution of the eigenvalue problem (6.1) results in the eigenvectors:

$$\mathbf{w} = \left\{-\frac{i}{2}, \frac{1}{2}\sqrt{\frac{H_{11}}{H_{22}}}, 0\right\}$$

and $w_3 = \{0,0,1\}$. The oscillation index is expressed as follows:

$$\epsilon = \frac{1}{2\pi} \ln\left(\frac{1-\beta}{1+\beta}\right), \tag{6.3}$$

where the first and second Dundurs' parameters are defined by

$$\alpha = \frac{\Sigma - 1}{\Sigma + 1} \quad \text{and} \quad \beta = \frac{H_{12}}{\sqrt{H_{11}H_{22}}}, \tag{6.4}$$

respectively, and

$$\Sigma = \frac{\left[\sqrt{s_{11}s_{22}}\right]_{\#2}}{\left[\sqrt{s_{11}s_{22}}\right]_{\#1}}.$$

The stresses σ_{22} and σ_{12} at a distance r in front of the crack tip at $\theta = 0$ (Fig. 6.1b) can be expressed as follows (Suo and Hill, 1990; Wang et al, 1992):

$$\sqrt{\frac{H_{22}}{H_{11}}}\sigma_{22} + i\sigma_{12} = \frac{Kr^{i\epsilon}}{\sqrt{2\pi r}} \tag{6.5}$$

and an associated pair of the relative crack surface displacements (jumps) Δ_1 and Δ_2 at a distance r behind the crack tip at $\theta = \pm\pi$, can be presented in the form:

$$\sqrt{\frac{H_{11}}{H_{22}}}\Delta_2 + i\Delta_1 = \frac{2H_{11}Kr^{\frac{1}{2}+i\epsilon}}{\sqrt{2\pi}(1+2i\epsilon)\cosh\pi\epsilon} \tag{6.6}$$

Here, $i = \sqrt{-1}$, $K = K_1 + iK_2 = |K|\, e^{i\psi}$ with K_1 and K_2 used instead of K_I and K_{II} adopted for homogeneous materials and the mode mixity phase angle ψ is specified as

$$\psi = \tan^{-1}\sqrt{\frac{H_{11}}{H_{22}}}\left(\frac{\sigma_{12}}{\sigma_{22}}\right) \tag{6.7}$$

To avoid oscillations in the mode mixity parameter, a characteristic length scale, $\hat{l}$ chosen in consistence with discussions in Hutchinson and Suo (1991) is usually introduced. Then, the non-oscillatory phase angle $\hat{\psi}$ is established as

$$\hat{\psi} = \tan^{-1}\sqrt{\frac{H_{11}}{H_{22}}}\left(\frac{\sigma_{12}}{\sigma_{22}}\right)\Bigg|_{r=\hat{l}} = \tan^{-1}\left(\frac{\Im m\{K\hat{l}^{i\epsilon}\}}{\Re e\{K\hat{l}^{i\epsilon}\}}\right), \tag{6.8}$$

where $K\hat{l}^{i\epsilon} = \hat{K}$ is a normalized complex SIF with ordinary units as those in homogeneous materials. The amplitudes of $\hat{K}$ and K are the same, but their phase angles are distinguished as $\hat{\psi} = \psi + \epsilon \ln \hat{l}$.

The ERR, $\mathcal{G}$ is related to the components of complex SIF as follows (Suo and Hill, 1990; Kuang-Chong, 1991):

$$\mathcal{G} = \frac{H_{11}}{4\cosh^2\pi\epsilon}\left(K_1^2 + K_2^2\right) \tag{6.9}$$

6.3 Numerical Evaluation of Interface Fracture Parameters

In this section, the numerical methods, which are appropriate for numerical solutions based on the FEM for obtaining the fracture parameters of an interfacial bimaterial system, are discussed.

6.3.1 Interaction Integral Method (IIM)

The interaction integral method is one of the most popular techniques to calculate complex SIFs by the FEM. This method is based on the Rice's J-integral which is identical to the ERR in LEFM. A common way to calculate the J-integral within the framework of the FEM is the use of the domain integral approach (Shih and Asaro, 1988). The 2-D domain form of the J-integral over the closed counter $C+C_+ + \Gamma + C_-$ around the crack tip (Fig. 6.1a) can be expressed as follows:

$$J = \int_A \left(W\mathbf{I} - \boldsymbol{\sigma} \cdot \frac{\partial \mathbf{u}}{\partial \mathbf{x}} \right) : \frac{\partial \mathbf{q}}{\partial \mathbf{x}} dA - \int_{C_+ + C_-} \mathbf{t} \cdot \frac{\partial \mathbf{u}}{\partial \mathbf{x}} \cdot \mathbf{q} d\Gamma, \tag{6.10}$$

where W is the strain energy; $\mathbf{u}$ and $\boldsymbol{\sigma}$ are the displacement and stress fields; A is the domain enclosed by the contour $C+C_+ + \Gamma + C_-$; $\mathbf{q}$ is a smooth weighting parameter that takes $\mathbf{q} = \mathbf{q}_1$ on Γ and is zero on C; $\mathbf{m}$ is the outward vector normal to the closed contour such that $\mathbf{m} = -\mathbf{n}$ on Γ and $\mathbf{t} = \mathbf{m} \cdot \boldsymbol{\sigma}$ on $C_+ + C_-$ if the surface traction on the crack flanks are accounted for. A geometrical interpretation of $\mathbf{q}$ is a virtual advancing of the crack tip in the local direction $\mathbf{q}_1$.

Following the finite element spatial discretization, the domain integral (6.10) is computed over a group of finite elements enclosed into the domain A (a ring around the crack tip in Fig. 6.1a).The integration is achieved by using the Gaussian quadratures for each element and consecutive summation, i.e.

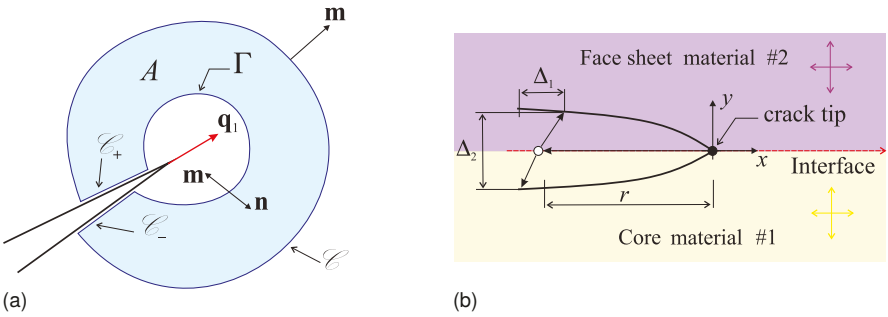

Fig. 6.1. Sketches of: (a) a closed contour $C + C_+ + \Gamma + C_-$ around the crack tip; (b) displacements of crack flanks at bi-material crack bounded by orthotropic materials.

$$J = \sum_{n=1}^{El} \left(\sum_{p=1}^{G} [f]^{(p)} |\mathbf{j}|^{(p)} \widetilde{w}_p \right)_n , \tag{6.11}$$

where n and p indicate that all the entities are associated with the n-th finite element of the area A and are determined at the p-th Gauss integration point; $[f]$ is the integrand in (6.10), $|\mathbf{j}|$ is the determinant of Jacobian matrix and $\widetilde{w}$ is the weight of the Gauss numerical quadrature. The domain integral is calculated by post-processing the results of finite element analysis.

The basic idea of the interaction integral method for calculating separated fracture modes involves superposing actual and auxiliary (*aux*) displacement and stress fields, where the auxiliary ones are assumed to be known a priori. The asymptotic Williams type' solutions of the corresponding material system regardless of the actual geometry can be used as the auxiliary field. Then, using the relation between the ERR and the SIF components (6.9), the interaction integral takes the form:

$$J_{int}^{M} = \frac{2}{H} \left(K_1 K_1^{aux} + K_2 K_2^{aux} \right), \quad \text{with} \quad H = \frac{4\cosh^2 \pi\epsilon}{H_{11}} \tag{6.12}$$

This formula is valid for each fracture mode $M = I, II$. On the other hand, the interaction integral for a straight crack can be expressed analogously to the J-integral definition in (6.10), i.e.

$$J_{int}^{M} = \int_A \mathbf{Q}^M : \frac{\partial \mathbf{q}}{\partial \mathbf{x}} dA \tag{6.13}$$

with the integrand $\mathbf{Q}^M$ given by

$$\mathbf{Q}^M = \boldsymbol{\sigma} : (\boldsymbol{\varepsilon}^{aux})^M \mathbf{I} - \boldsymbol{\sigma} \cdot \left(\frac{\partial \mathbf{u}^{aux}}{\partial \mathbf{x}} \right)^M - (\boldsymbol{\sigma}^{aux})^M \cdot \frac{\partial \mathbf{u}}{\partial \mathbf{x}} \tag{6.14}$$

Since the interaction integral is formulated similar to the J-integral in (6.10), the domain integration approach identical to that in (6.11) can be applied to the numerical computation of the integral in (6.13).

Finally, making a judicious choice of the auxiliary stress intensity factors and computing auxiliary displacement and stress fields associated with them, the separated stress intensity factors can be evaluated as follows:

$$K_M = \frac{H}{2K_M^{aux}} J_{int}^{M} \tag{6.15}$$

6.3.2 Crack Surface Displacements (CSD) Method

The CSD method is based on the approach proposed by Smelser (1979). In accordance with this method, the complex SIF components are determined by the amplitude and phase angle of K which are calculated using the displacements at the crack faces close to the crack tip (Fig. 6.1b).

The method has an advantage for computing the SIF components in the context of the FEM since the displacement field is a direct outcome of the finite element analysis. Thus, in contrary to the IIM, the CSD method does not require the retrieval of strains and stresses. Using (6.6) in conjunction with the expressions for the mode-mixity parameter (6.8) and the ERR (6.9), it yields the formulae to compute the fracture characteristics as follows (Kardomateas et al, 2013):

$$\hat{\psi} = \tan^{-1}\left(\sqrt{\frac{H_{11}}{H_{22}}}\frac{\Delta_1}{\Delta_2}\right) - \epsilon \ln\left(\frac{r}{\hat{l}}\right) + \tan^{-1} 2\epsilon \tag{6.16}$$

and

$$\mathcal{G} = \frac{H_{11}|K|^2}{4\cosh^2 \pi\epsilon} = \frac{\pi(1+4\epsilon^2)}{8H_{11}\left(r/\hat{l}\right)}\left(\frac{H_{11}}{H_{22}}\Delta_2^2 + \Delta_1^2\right), \tag{6.17}$$

where

$$\Delta_j = u_j(r,\pi) - u_j(r,-\pi), \quad j = 1,2$$

represents the relative crack flank displacements (shearing and opening modes) at distance r behind the crack tip, H_{11} and H_{22} are components of the matrix $\mathbf{H}$.

Thus, in accordance with the CSD method, the nodal displacements of finite elements, whose faces are adjacent to the opposite crack flanks, are extracted from the finite element results to compute the ERR and phase angle at different distances r close to the crack tip. However, approaching the crack tip, the values of ERR and phase angle tend to be incorrect due to the singular nature of the relative displacements Δ_1 and Δ_2 at $r \to 0$. Instead, the ERR and phase angle are estimated by linear extrapolation of their values in a chosen interval of r to the crack tip (Ryoji and Sang-Bong, 1989). The nodal displacements in the neighborhood of the region - $r/\hat{l}$ about $10^{-2} - 10^{-3}$ typically provides a good estimate of $\mathcal{G}$ and $\hat{\psi}$ (Smelser, 1979). Finally, the results can be expressed in terms of stress intensity factors:

$$\begin{aligned} K_1 &= \Re e\{K\hat{l}^{i\epsilon}\} = |K|\cos\psi \\ K_2 &= \Im m\{K\hat{l}^{i\epsilon}\} = |K|\sin\psi, \end{aligned} \tag{6.18}$$

where $\psi = \hat{\psi} - \epsilon \ln \hat{l}$ for a given reference length, $\hat{l}$. A free choice of $\hat{l}$ in the determination of ψ is proven by fulfilling a simple transformation rule from one value to another (Suo and Hutchinson, 1990): $\psi_2 = \psi_1 + \epsilon \ln\left(\hat{l}_2/\hat{l}_1\right)$ with ψ_1 and ψ_2 associated with l_1 and l_2, respectively.

It is worth mentioning that since the analytical expressions (6.16) and (6.17) allow extracting the fracture parameters from numerical displacement data, the accuracy of this process is dependent upon the amount of data available along the crack flanks in the vicinity of the tip. Hence, a fine enough mesh in the region around the crack tip is required in the FEM calculations. Also, some accuracy difficulties may be encountered in determining the ERR and phase angle from the FEM displacements for models with high overall stiffness or when the angles are small (Smelser, 1979). The first issue can be overcome by using the J-integral and correlating the results of the both methods, whereas the second one is not critical as long as the interface bond is weak relative to the two adjoining materials. When this is the case, the crack will

most likely propagate along the interface with dominating failure mode I i.e. the angle of the stress intensity factor is not so important.

6.4 Numerical Solutions

In this section, we present the results of numerical evaluations of the fracture parameters of DCB-UBM, DCB and SCB sandwich specimens used for the interfacial bond strength assessment of sandwich panels. The calculations are carried out using the finite element code ABAQUS (2016). The interaction integral method is a built-in option of the package, but it is applied to bi-material interfaces consisting of two isotropic dissimilar materials only. The CSD method is programmed as an add-on subroutine in Matlab environment and can be utilized for orthotropic bi-material configurations. The subroutine extracts the displacements at given nodal sets from the ABAQUS' result database file and, then, computes the required values (Burlayenkoal, et al, 2018, 2019a). The numerical results are compared with known analytical solutions or experimental data, when these are available in the literature.

6.4.1 DCB-UBM Sandwich Specimen

A DCB-UBM sandwich beam shown in Fig. 6.2a is selected as a first example. The DCB-UBM test method was first used in Sorensen et al (2006) for evaluating the interface strength of laminated composites and, was later extended to sandwich materials (Saseendran et al, 2018). In this test, the DCB specimen's cracked edges are subjected to uneven bending moments, M_1 and M_2 (both being defined per unit specimen width, b), while the intact end of the specimen is fixed and generates the reactive moment $M_0 = M_1 + M_2$, as illustrated in Fig. 6.2a. The DCB-UBM test allows a variety of mixed mode I/II states by changing the ratio of the moments applied to the specimen, $MR = M_1/M_2$. Considering this, the crack is open at a negative ratio $MR < 0$, while a positive ratio $MR > 0$ generates sliding between the crack flanks. Also, it is known that the test enables to produce the crack length-inde-

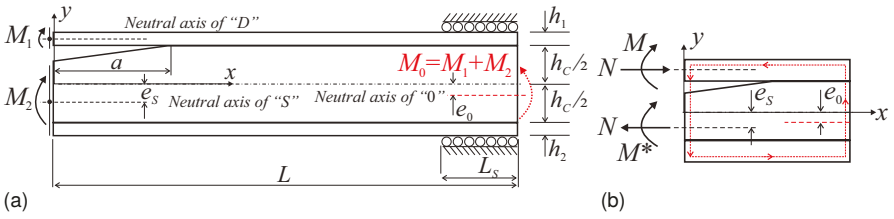

Fig. 6.2. DCB-UBM sandwich specimen: (a) geometry and loading; (b) local force and moment resultants.

pendent ERR and a constant mode mixity, when the moment ratio MR does not change during the crack growth.

The ERR can analytically be determined using the specimen geometry, elastic properties and applied external bending moments. The Euler-Bernoulli theory is utilized to model both the intact end of the specimen and each of the cracked edges. In the case of orthotropic face sheets and/or core, the principal material axes are aligned with the reference coordinate axes of the specimen and Young's moduli corresponding to the specimen axial rigidity are used in the formulation. The J-integral calculated along the outer boundaries of the specimen (Fig. 6.2b) leads to the following expression (Burlayenko et al, 2019c):

$$\mathcal{G}^{DCB-UBM} = \frac{1}{2b}\left\{\frac{N^2}{(EA)_D} + \frac{N^2}{(EA)_S} + \frac{M^2}{(EI)_D} + \frac{M^{*2}}{(EI)_S}\right\}, \tag{6.19}$$

where $N = \gamma_2 M_0$, $M = M_1 - \gamma_3 M_0$ and

$$M^* = N\left(e_s + \frac{h_c}{2} + \frac{h_1}{2}\right) - M$$

are the equivalent axial load and bending moments, respectively, with

$$\gamma_2 = \frac{(EA)_D}{(EI)_0}\left(e_0 + \frac{h_c}{2} + \frac{h_1}{2}\right) \quad \text{and} \quad \gamma_3 = \frac{(EI)_D}{(EI)_0};$$

the parameters e_0 and e_s locate neutral axes of the intact part of specimen and the substrate, Fig. 6.2; $(EA)_i$ and $(EI)_i$ are generalized axial and flexural rigidities of the debonded portion "D", substrate "S" and intact part "0" of the specimen, i.e. $i = D, S, 0$. It should be noted that the expression of ERR (6.19) is applicable to DCB sandwich samples subjected to bending moments only, and it does not account for shear and root rotations (Thouless, 2018).

The fracture analysis was carried out for the DCB-UBM specimen with glass/epoxy composite face sheets of thicknesses $h_1 = h_2 = 2.4$ mm and a PVC H 100 core of thickness $h_c = 50$ mm. The resin rich layer between the face sheets and the core is considered to be a zero thickness, i.e. we neglect its influence on the interfacial fracture behaviour at all. The material properties of the sandwich specimen constituents are summarized in Table 6.1. The specimen of total length $L = 270$ mm with pre-crack of length $a = 90$ mm and a fixed end of length $L_s = 27$ mm was considered. It is assumed that the principal axes of the orthotropic materials of face sheet and core of the specimen are aligned with the co-ordinate axes, Fig. 6.2a. Also, the Young's moduli along the x-axis of the given orthotropic materials are adopted as the effective moduli for determining the generalized stiffness in (6.19).

A 2-D finite element model of the DCB-UBM specimen is developed using eight-node reduced integration plane strain finite elements (CPE8R) available in ABAQUS, Fig. 6.3. The finite element mesh contains a refinement in the vicinity of the crack-tip as shown in Fig. 6.3. In the calculations, the bending moments are applied to the DCB-UBM specimen edges at the points of the neutral axes of each subregion of the cracked part, Fig. 6.2a. Coupling kinematic constraints (ABAQUS, 2016) between

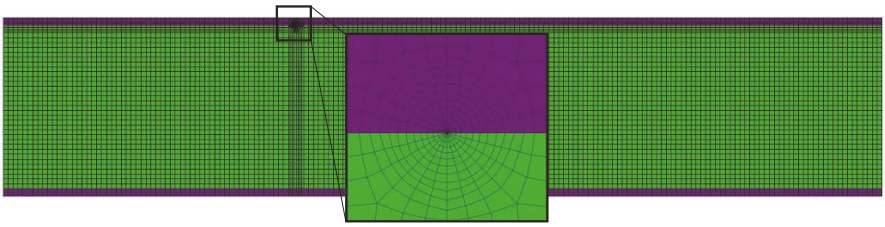

Fig. 6.3. A 2-D finite element model of the DCB-UBM sandwich specimen.

the set of nodes on the edge and the point of neutral axis are used to enforce equal rotation of the entire edge. The debonding in the specimen is modelled by a real gap of $\frac{h_1}{100}$ between the separated face sheet and core. The contact and friction conditions analogous to those in Burlayenko and Sadowski (2018) are introduced between the faces of the appropriate finite elements located along the pre-cracked bi-material interface.

To demonstrate the performance of the developed finite element model, different moment ratios, MR are considered in the calculations. Both the J-integral option of ABAQUS (2016) and the CSD method that post-processes the finite element results using the add-on Matlab-subroutine are utilized for computing the fracture characteristics. In all the calculations, the bending moments induced nearly the same ERR for each loading case. The values of ERR, $\mathcal{G}$ computed numerically were compared with those found using the analytical formula (6.19) and the semi-analytical expression deduced in Kardomateas et al (2013). Good agreement between all the solutions has been achieved as seen in Table 6.2, where the phase angle ψ and the complex SIF components found with the CSD method are presented as well.

The contour plots of the stress tensor components associated with different moment ratios, MR listed in Table 6.2 are illustrated in Fig. 6.4, where the first row

Table 6.1
Material properties of the sandwich specimens.

Constituents	Material constants
Glass/Epoxy face sheet	$E_x = E_z = 16.5$ GPa; $E_y = 3.8$ GPa; $G_{xy} = G_{xz} = 1.3$ GPa; $G_{yz} = 6.6$ GPa; $\nu_{xy} = 0.05$; $\nu_{xz} = \nu_{yz} = 0.25$; $\rho = 1650$ kgm^{-3}
E-Glass/Epoxy face sheet	$E_x = 27.6$ GPa; $E_y = 25.2$ GPa; $E_z = 3$ GPa; $G_{xy} = 2.2$ GPa; $G_{yz} = G_{xz} = 1.2$ GPa; $\nu_{xy} = 0.24$; $\nu_{xz} = 0.12$; $\nu_{yz} = 0.06$; $\rho = 1800$ kgm^{-3}
Aluminium face sheet	$E_x = E_y = E_z = 69.5$ GPa; $\nu_{xy} = \nu_{xz} = \nu_{yz} = 0.3$; $\rho = 2700$ kgm^{-3}
PVC H 80 foam core	$E_x = E_y = E_z = 80$ MPa; $G_{xy} = G_{xz} = G_{yz} = 27.3$ MPa; $\nu_{xy} = \nu_{xz} = \nu_{yz} = 0.25$; $\rho = 80$ kgm^{-3}
PVC H 100 foam core	$E_x = E_y = E_z = 105$ MPa; $G_{xy} = G_{xz} = G_{yz} = 39.8$ MPa; $\nu_{xy} = \nu_{xz} = \nu_{yz} = 0.325$; $\rho = 100$ kgm^{-3}

of the images corresponds to σ_{11}, the second and third ones show σ_{22}, and σ_{12}, respectively. A complicated nature of the near-tip stress field is clearly observed here. One can see that the shear stress exists in the vicinity of the crack regardless of the loading cases as shown in the third row of Fig. 6.4. This is an apparent evidence of the mode mixity conditions being expected in sandwich structures. By comparing the values of the total ERR in Table 6.2, which are calculated by the FEM accounting for shear stress and by the analytical formula (6.19) neglecting it, one can conclude that the shear stress does not influence much on the total value of the ERR in this case. However, the sign of the shear stress ahead of the crack defines a favourable direction of interface crack propagation in the bi-material interface as mentioned in Adams et al (2012) and shown in Burlayenko et al (2019b).

6.4.2 DCB Sandwich Specimen

The second example considers symmetric ($h_1 = h_2 = h_f$) sandwich beam-like specimens exploited in the DCB test method. A scheme of the DCB test is illustrated in Fig. 6.5a. In this test, two piano hinges are usually used to transfer the loading to the edges of the specimen's cracked region. The DCB sandwich specimen is subjected to an opening displacement by applying to the grip plates either two opposite transverse loads or an upward load and appropriate boundary constraints. The asymmetry of the specimen caused by the fact that the lower part (below the crack plane) being more rigid in flexure than the upper one (above the crack plane) may result in a slight rotation of the specimen at large opening displacements as shown in Fig. 6.5b, but usually such a rotation tends to be small in actual tests (Avilés and Carlsson, 2008).

The total ERR, generated by the interface crack during DCB testing can analytically be evaluated. Avilés and Carlsson (2008) used a model that considers the upper face sheet as a beam partially supported by an elastic foundation representing

Table 6.2
Calculations of the ERR and the phase angle with respect to the moment ratio MR.

	M_1 Nmm	75.6	103.42	123.4	104.13	73.8
	M_2 Nmm	-1512.2	-1034.2	-123.4	1041.3	1476
	MR	-0.05	-0.1	-1.0	0.1	0.05
ERR,	$\mathcal{G}^{FEM}$ N/mm	0.399	0.399	0.403	0.399	0.377
	$\mathcal{G}^{(6.19)}$ N/mm	0.398	0.398	0.402	0.400	0.375
	$\mathcal{G}^{\text{Kardomateas et al (2013)}}$ N/mm	0.351	0.363	0.376	0.365	0.332
Phase angle,	ψ^{FEM} deg.	30.26	11.31	-17.16	-51.87	-70.71
SIFs,	$\Re e\{K\hat{h_1}^{i\epsilon}\}$ N/mm$^{\frac{3}{2}}$	9.652	10.96	10.74	6.914	3.585
	$\Im m\{K\hat{h_1}^{i\epsilon}\}$ N/mm$^{\frac{3}{2}}$	5.631	2.192	3.313	8.809	10.24

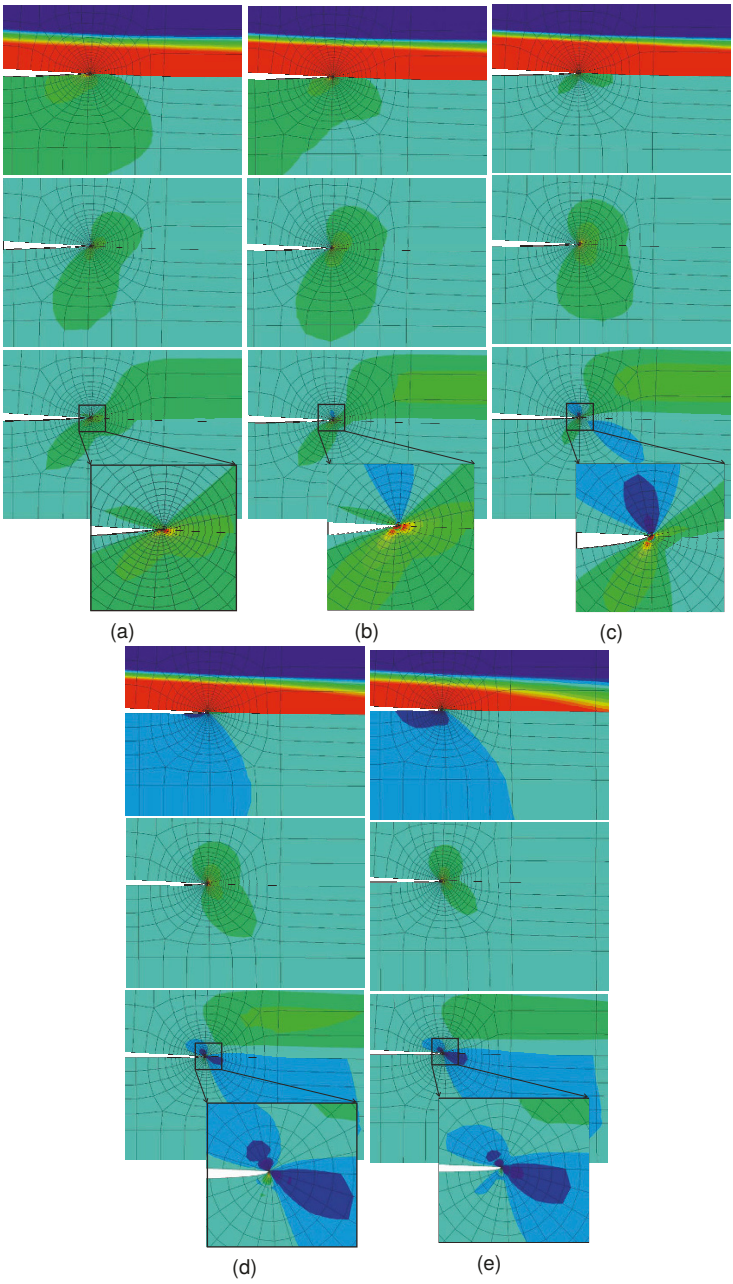

Fig. 6.4. Contour plots of the stress components at the crack tip of the DCB-UBM specimen w.r.t. the moment ratio MR equal to: (a) -0.05; (b) -0.1; (c) -1; (d) 0.1; and (e) 0.05.

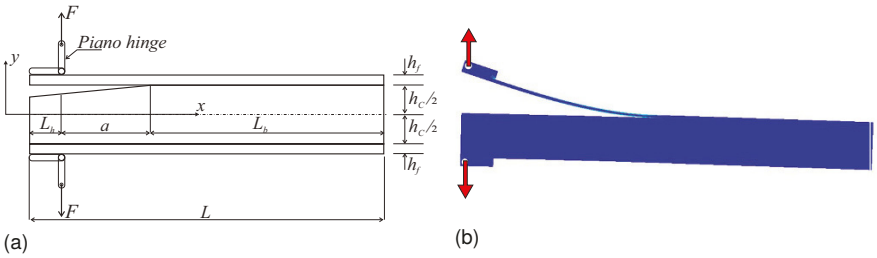

Fig. 6.5. Double Cantilever Beam sandwich specimen: (a) a schematic test; and (b) a deformed configuration.

a core. The model formulation was based on the assumptions of the Euler-Bernoulli beam theory and the Winkler elastic foundation theory for describing the deformation of the upper face sheet and the core of the DCB specimen, shown in Fig. 6.5b, respectively. The final expression of the ERR has a form:

$$\mathcal{G}^{DCB} = \frac{F^2}{2b^2}\left\{\frac{1}{G_{xz}h_c} + \frac{a_0^2}{(D - B^2/A)} + \frac{12}{E_f h_f^3}\left(a_0^2 + 2a_0\eta^{1/4} + \eta^{1/2}\right)\right\}, \qquad (6.20)$$

where the initial crack length $a = a_0$, the parameter $\eta = bh_f^3 E_f/(3K)$ and the elastic foundation coefficient $K = 2bE_c/h_c$. The 1-D extensional, coupling and bending stiffness coefficients A, B and D are computed as

$$A = E_f h_f + E_c h_c, \quad B = \frac{h_f h_c}{2}(E_c - E_f) \text{ and}$$
$$D = \frac{1}{12}\left\{E_f(h_f^3 + 3h_f h_c^2) + E_c(h_c^3 + 3h_f h_c^3)\right\}$$

The finite element model similar to that used in the fracture analysis of the DCB-UBM specimen (Fig. 6.3) was adopted for the numerical calculations of the fracture parameters in the DCB specimens. To accurately reproduce the specific loading conditions in the finite element model, the hinges, modelled as rigid bodies, were linked to the face sheets of the sandwich beam using the `TIE` constraints (ABAQUS, 2016). Moreover, the external concentrated forces were applied to points in the centres of the hinge holes. Each the point was connected to the hole contour using Multi-point Constraints (MPCs). This type of constraint allows a hinge rotation relatively to the point of force application, i.e. it simulates the real conditions of the laboratory testing, Fig. 6.5b.

In the finite element predictions, DCB sandwich specimens of length $L = 250$ mm and width $b = 25$ mm with a PVC H 80 foam core of thickness $h_c = 25$ mm and either e-glass/epoxy composite or aluminium face sheets of thickness, h_f ranging from 0.1 mm to 10 mm at different pre-crack lengths a=30,50,70,90 and 110 mm are analysed. The properties of the sandwich specimen constituents are shown in Table 6.1. The comparisons of the ERR computed by resolving a 2-D elasticity problem

with the FEM in conjunction with the J-integral method and obtained using the analytic expression (6.20) based on the classical beam theory are presented in Fig. 6.6. The plot illustrates a scattering of relative errors between both the results

$$\Delta\mathcal{G} = \frac{|\mathcal{G} - \mathcal{G}^{DCB}|}{\mathcal{G}} \times 100\%$$

with respect to appropriate linear trend lines depending on the face sheet thickness and the pre-crack length. It is found that the analytical predictions mainly overestimate the numerical ones, but the differences between them do not exceed 50% and the error tends to decrease with thickening the face sheet. Also, the findings observed in Fig. 6.6 show that the differences between the two solutions are smaller for the specimens with composite face sheets (Fig. 6.6a) than with stiffer aluminium ones, i.e. for a lower material ratio, E_f/E_c. Herewith, the differences become smaller with increasing the pre-crack length in both types of the specimens. Thereby, the numerical results clearly demonstrate the limitations of the analytic formula (6.20) and justify the importance of accounting for shear deformation in the vicinity of the crack tip for accurate calculations of the ERR.

The other validation of the finite element model is done by comparing numerically computed ERRs and those obtained experimentally in Avilés and Carlsson (2008). Two types of DCB sandwich specimens denoted as 'thick DCB' and 'thin DCB' are considered. All details related to these two tests can be found in the mentioned source and the references cited there. The results of the comparison are displayed in Fig. 6.7 for a normalized value of the ERR,

$$G^* = \frac{G}{F^2}.$$

It is seen that the finite element predictions are satisfactory close to the measured data for all the crack lengths studied in both the specimens. Also, it is obvious that the trends of changing the ERRs with increasing the crack length observed

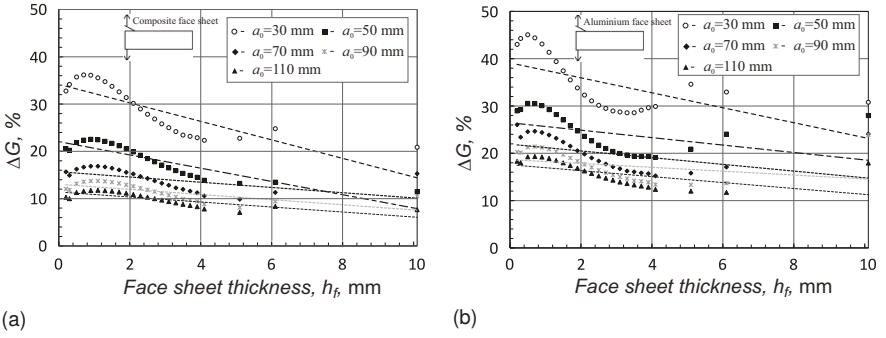

Fig. 6.6. The variation of relative errors $\Delta\mathcal{G} = \frac{|\mathcal{G}-\mathcal{G}^{DCB}|}{\mathcal{G}} \times 100\%$ vs. the face sheet thickness h_f for different pre-crack lengths in the DCB test with: (a) composite face sheets; and (b) aluminium face sheets.

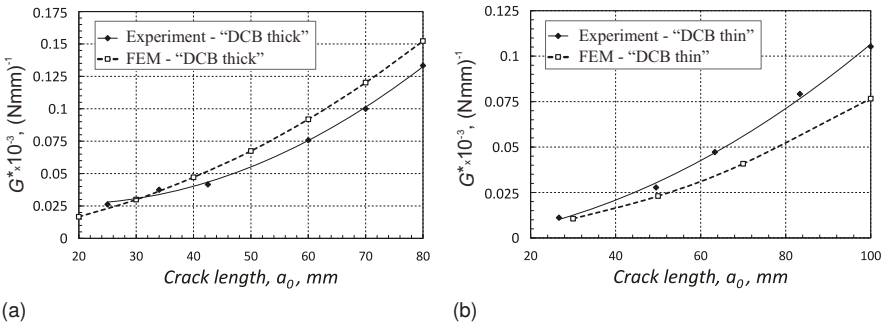

Fig. 6.7. Comparison between numerical and experimental ERRs vs. crack length for DCB sandwich specimens: (a) thick sample; and (b) thin sample.

in the experiments and predicted by the finite element analysis show quite similar behaviours. Hence, one can conclude that the computational models can accurately represent the actual DCB tests.

The ERR and the phase angle, computed by both the IIM and the CSD method for a 150 mm length and 27 mm width DCB sandwich specimen with pre-crack of a_0 = 50 mm, which is made up of the PVC H-100 core of thickness h_c = 38 mm and the e-glass/epoxy composite face sheets of thickness h_f =2.4 mm, subjected to a unit load are presented in Table 6.3. It is seen that although the IIM uses effective elastic properties reduced to isotropic materials instead of actual orthotropic ones, both the numerical techniques give quite close results. Also, the calculated fracture characteristics clearly exhibit the dominated mode I deformation of the DCB specimen at the given material and geometrical parameters. The distribution of near-tip stress fields in the DCB specimen is demonstrated in Fig. 6.8. The plots show that the maximum longitudinal normal stress is primarily developed in the upper (debonded) face sheet due to its high in-plane and bending resistance, Fig. 6.8a, whereas the transverse normal stress is the biggest in the region around the crack tip, Fig. 6.8b. In addition, the shear stress exists at the crack tip, Fig. 6.8c. However, this stress component is smaller about one order of magnitude than the transverse normal stresses in the same region. Despite its relatively small magnitude, the sign of shear stress in the vicinity of the crack tip defines the orientation of presumed crack growth direction (Adams et al, 2012). As seen in Fig. 6.8c, the shear stress

Table 6.3
Calculations of the ERR, SIFs and phase angle for DCB and SCB specimens.

Specimen type	Method	$\mathcal{G}$ N/mm	$\Re e\{K\hat{h}_1^{i\epsilon}\}$ N/mm$^{\frac{3}{2}}$	$\Im m\{K\hat{h}_1^{i\epsilon}\}$ N/mm$^{\frac{3}{2}}$	ψ deg.
DCB	IIM	67.76e-6	0.1299	-0.0321	-13.93
	CSD	67.21e-6	0.1356	-0.0448	-18.29
SCB	IIM	12.39e-6	0.0689	-0.011	-9.08
	CSD	12.01e-6	0.0586	-0.015	-13.03

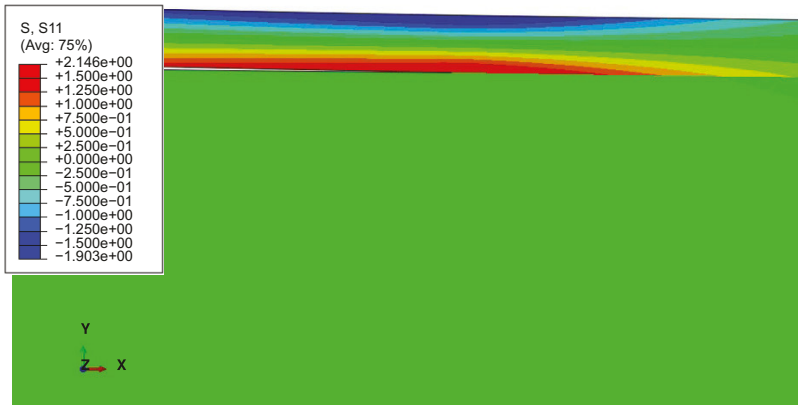

(a)

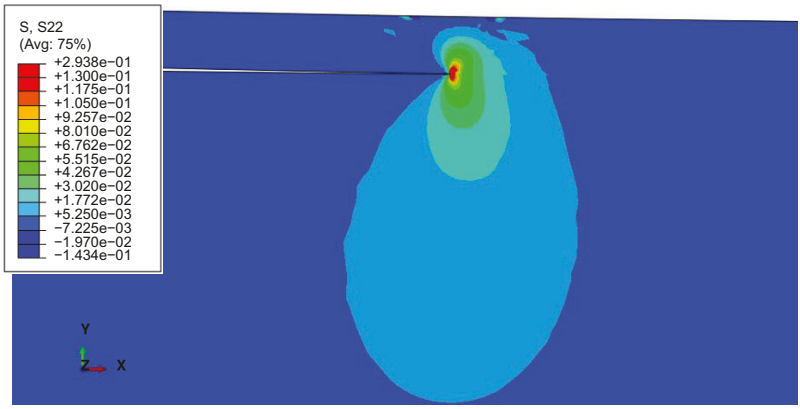

(b)

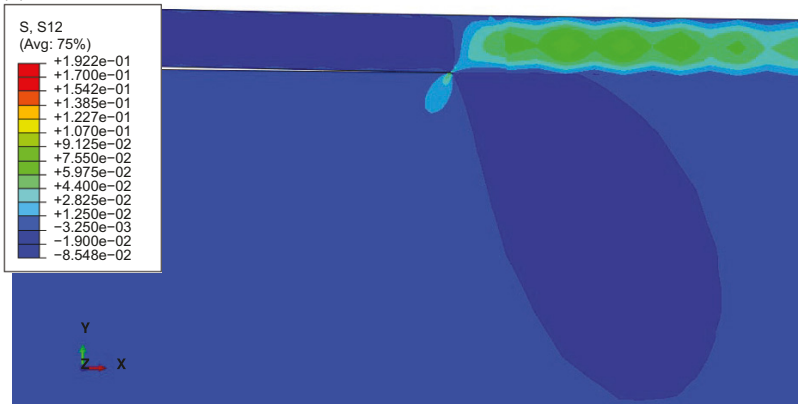

(c)

Fig. 6.8. Stress distribution in front of the debonding in DCB specimen: (a) longitudinal normal stress σ_{11}; (b) transverse normal stress σ_{22}; and (c) in-plane shear stress σ_{12}.

arisen in the area around the crack tip is strongly negative that confirms the finding for a negative phase angle, ψ observed in Table 6.3. This value predicts the crack propagation direction either into the face sheet material or along the face sheet/core interface during this test method. The latter crack growth path is more likely due to a weaker crack resistance of the face sheet/core interface compared with the face sheet strength.

6.4.3 SCB Sandwich Specimen

The last example is a SCB sandwich specimen, which presents the second class of test methods generating dominated mode I fracture by peeling the face sheet from the core. A SCB test method with given boundary conditions and schematic loading is illustrated in Fig 6.9a. As seen, only one upward force, F is applied to the specimen through a steel hinge mounted on the upper debonded face sheet, while the lower one is affixed to a rigid base. Moreover, to provide an accurate interface toughness measurement and to ensure that bending is the primary form of loading, the dimensions of the SCB specimen and the load rod length, h_F have to satisfy sizing requirements defined in Ratcliffe and Reeder (2011).

An analytical estimation of the total ERR $\mathcal{G}^{SCB}$ can be deduced from a kinematic analysis of the SCB sandwich sample (Fig. 6.9b) within the elastic foundation approach. Then, the final expression can be written as follows (Rinker et al, 2011):

$$\mathcal{G}^{SCB} = \frac{4\lambda F^2}{2bK}\left\{\lambda^3 a_0^2 + 2\lambda^2 a_0 + \lambda + \frac{K}{4b\lambda k G_{xz}^f h_f}\right\}, \tag{6.21}$$

where the parameter

$$\lambda = \left(\frac{K}{4D_f}\right)^{1/4}$$

with

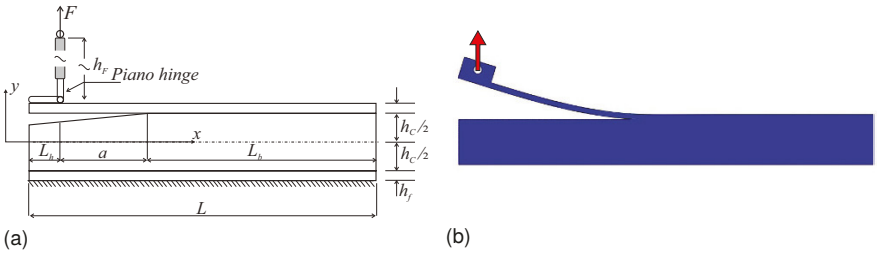

Fig. 6.9. Single Cantilever Beam sandwich specimen: (a) a schematic test; and (b) a deformed configuration.

$$D_f = \frac{bh_f^3}{12}$$

and the foundation coefficient

$$K = \frac{bE_c}{h_c}$$

is identical to that in (6.20).

In the context of comparative studies, both the analytic expression (6.21) and the general formula of LEFM (6.6) are used to calculate the ERR for a variety of SCB specimens distinguished by the pre-crack length and the face sheet thickness. The SCB specimens of a 250 mm length made up of a 50 mm thick PVC H-80 foam core and either glass/epoxy composite or aluminium face sheets of the thickness varying from 0.1 to 10 mm are analysed. The comparisons, presented by relative errors between the results computed with FEM and those found analytically

$$\Delta\mathcal{G} = \frac{|\mathcal{G} - \mathcal{G}^{SCB}|}{\mathcal{G}} \times 100\%$$

the same as in Sect. 6.4.2, are shown in Fig. 6.10. Analogously to the predictions for the DCB specimens, it was found out that the approximate analytic formula (6.21) for the SCB specimens also mainly overestimates the ERR, especially it is apparent for short pre-cracks, but the maximal deviation does not exceed 50% in our study again. Herewith, the aluminium-PVC material configuration corresponding to a higher E_f/E_c ratio leads to bit larger differences than those in the composite-PVC system with a lower E_f/E_c ratio. This is similar to the results observed for DCB specimens considered in the previous example. Also, the errors are less for longer pre-cracks and thicker face sheets.

The comparison of the ERR values over a range of crack lengths, which are predicted with the finite element model and those known from experimental studies available in Li and Carlsson (1999), is illustrated in Fig. 6.11. The SCB specimens, tested in Li and Carlsson (1999) as tilted sandwich debond (TSD) samples at the

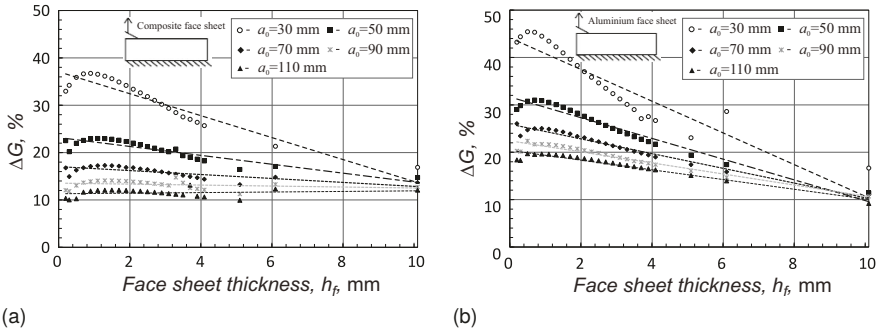

Fig. 6.10. The variation of relative errors $\Delta\mathcal{G}$ vs. the face sheet thickness h_f for different pre-crack lengths in the SCB test with: (a) composite face sheets; and (b) aluminium face sheets.

zero tilt angle, are considered for this comparative study. Mechanical properties and dimensions of the specimens as well as the details of laboratory testing can be found in the original reference. From Fig. 6.11 one can see that the dimensionless ERRs,

$$\mathcal{G}^* = \mathcal{G}\frac{E_f h_f^3}{(Fb)^2}$$

obtained numerically and the experimental values correlate quite well between each other. This confirms high-fidelity modelling results which are provided by the finite element models developed for the SCB sandwich specimens.

In Table 6.3, the finite element calculations performed for obtaining the ERR, SIFs and phase angle of a 210 mm length and 38 mm width SCB sandwich specimen consisting of 3.6 mm thick glass/vinylester face sheets bonded to a 50 mm thick PVC H-100 foam core are summarized for the case of unit transverse force and pre-crack length of $a_0 = 50$ mm. One can see that the results provided by the IIM approach and the SCD method are in good agreement similar to the case of the DCB specimen. The distribution of near-tip stress components, associated with the deformed state of this SCB specimen is plotted in Fig. 6.12. The analysis shows that the normal longitudinal and transversal stresses have profiles close to those observed in the DCB specimen (Fig. 6.8a and b), while the magnitude of the shear stress is visibly smaller than that in the DCB specimen (Fig. 6.8c). The reason of such similarity is that the face sheets of both the specimens behave in the same manner under the applied upward force, but the difference in the shear stresses is due to additional contribution of bending moment and shear force induced by a downward force acting on the lower part (below the crack plane) of the DCB sample. Hence, it is reasonable to expect that such the deformation state with extra shear and normal stresses at the crack tip can give rise to a more complicated cracking behaviour in the DCB specimen. Thus, the SCB specimen is able to produce dominated mode I deformation conditions with less limits than the DCB sample. This conclusion correlates with a smaller negative phase angle in the SCB test sample compared with the DCB specimen for the given face sheets and core materials and specimens' geometries as displayed in Table 6.3.

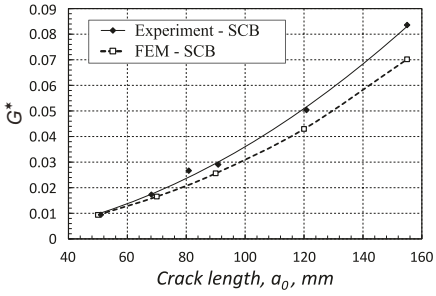

Fig. 6.11 Comparison between numerical and experimental ERRs vs. crack length for the SCB sandwich specimen.

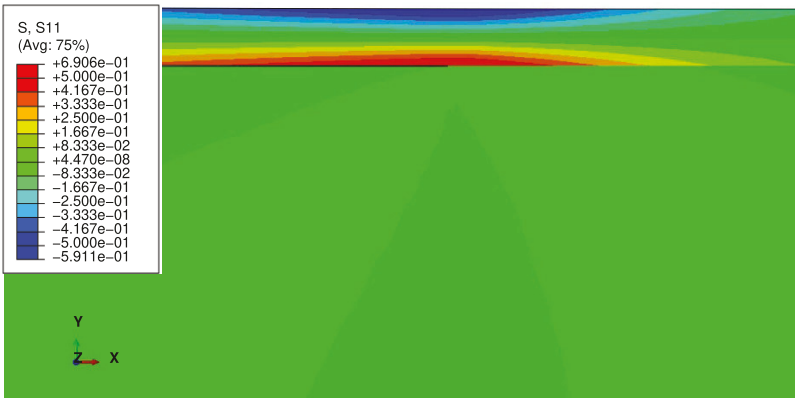

(a)

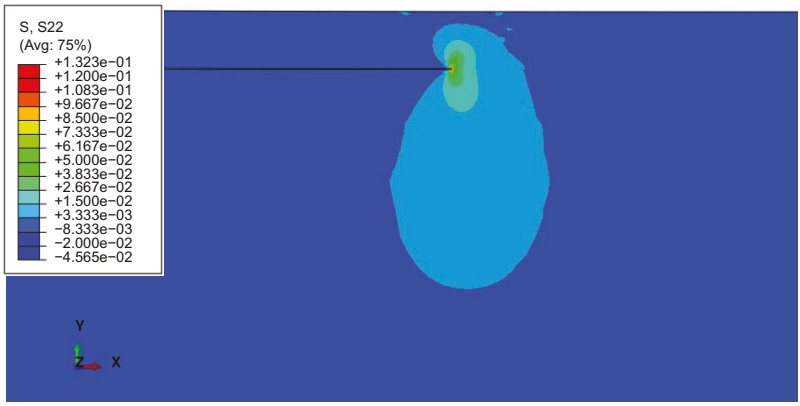

(b)

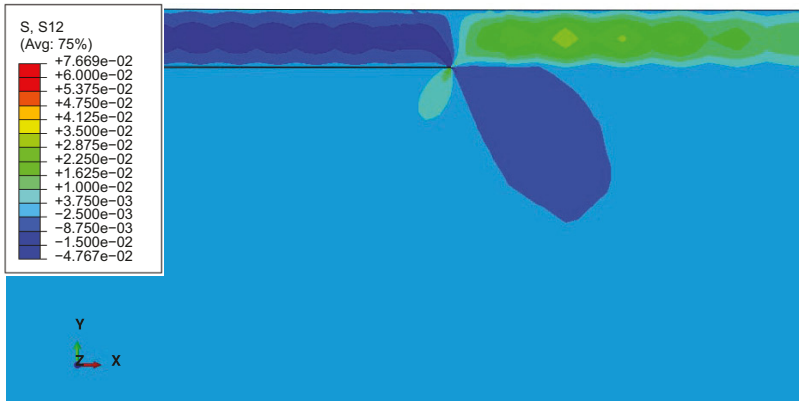

(c)

Fig. 6.12. Stress distribution in front of the debonding in SCB specimen: (a) longitudinal normal stress σ_{11}; (b) transverse normal stress σ_{22}; and (c) in-plane shear stress σ_{12}.

6.5 Conclusions

In this research, efforts have been focused on evaluating the fracture parameters in virtual tests related to the assessment of face sheet-to-core interface strength in sandwich panels. Both analytical methods based on beam-like models and two-dimensional finite element analyses with ABAQUS have been applied to the computation of ERR, SIFs and phase angle in popular DCB-UBM, DCB and SCB sandwich fracture specimens. The numerically obtained results have been extracted from the finite element solutions using two techniques such as the IIM and the CSD method, which are suitable for analysing a bi-material configuration of the sandwich panel interfaces in perspective of the evaluation of mode mixity. Also, the use of these methods in finite element predictions is very efficient since they have a straightforward finite element formulation that allows one exploiting a whole power of general purpose finite element packages like the ABAQUS code.

The parametric studies in the 2-D fracture analysis of the sandwich specimens made up of either aluminium or various composite laminated face sheets and PVC foam core of different thicknesses have been carried out. Results received from the finite element simulations of all the specimens were compared with those obtained by the analytical approximate formulae and the experimental data available in the literature for DCB and SCB fracture tests. Generally, good correlation between the results has been observed. Evaluating the fracture parameters of the hypothetical sandwich specimens, it was found that the shear stress exists in the vicinity of the crack tip regardless of the specimen type and the material and geometrical configurations of those specimens. Hence, it has been recognised that the mode mixity is an inherent characteristic of sandwich panels' deformed state. This characteristic should be known a priori to accurately estimate the strength of the face sheet-to-core interface and to simulate the debonding fracture along an appropriate crack growth path in sandwich panels. In turn, the crack path can be predicted based on a mode mixity fracture criterion, which could be known after performing a comprehensive actual and virtual test campaign.

Finally, it needs to mention that although the present results are demonstrated only for the selected three sandwich samples, the 2-D finite element techniques used in this research can be applied to virtual tests of sandwich specimens of any other geometry and boundary conditions. Thus, the results presented in the paper may provide a benchmark for studying the considered DCB-UBM, DCB and SCB sandwich fracture specimens and, on the other hand, they may guide further research associated with the assessment of interfacial strength of sandwich panels.

Acknowledgements The first author would like to mention that this research has been conducted during his stay at the Institute of Mechanics of Otto-von-Guericke-Universität Magdeburg, which was supported by the German Academic Exchange Service (DAAD) Funding Programme ID No. 57440915.

References

ABAQUS (2016) User's manual, ver. 2016. Dassault Systémes Simulia Corp., Providence, RI, USA

Adams DO, Nelson J, Bluth Z (2012) Development and evaluation of fracture mechanics test methods for sandwich composites. In: Proceedings of the 2012 Aircraft Airworthiness and Sustainment Conference, 2-5 April 2012, Baltimore, MD, US

Altenbach H, Altenbach J, Kissing W (2018) Mechanics of Composite Structural Elements, 2nd edn. Springer

Andrews MG, Massabò R (2007) The effects of shear and near tip deformations on energy release rate and mode mixity of edge-cracked orthotropic layers. Engineering Fracture Mechanics 74(17):2700 – 2720

Avilés F, Carlsson LA (2008) Analysis of the sandwich DCB specimen for debond characterization. Engineering Fracture Mechanics 75(2):153 – 168

Beuth JL (1996) Separation of crack extension modes in orthotropic delamination models. International Journal of Fracture 77:305 – 321

Bruno D, Greco F (2001) Mixed mode delamination in plates: a refined approach. International Journal of Solids and Structures 38(50):9149 – 9177

Burlayenko VN, Sadowski T (2011a) Dynamic analysis of debonded sandwich plates with flexible core - numerical aspects and simulation. In: Altenbach H, Eremeyev VA (eds) Shell-like Structures, Springer, Heidelberg, Advanced Structured Materials, vol 15, pp 415 – 440

Burlayenko VN, Sadowski T (2011b) Numerical modeling of sandwich plates with partially dedonded skin-to-core interface for damage detection. In: DeRoeck G, Degrande G, Lombaert G, Müller G (eds) Proceedings of the 8th International Conference on Structural Dynamics (EURODYN), Leuven, Belgium, pp 2242–2249

Burlayenko VN, Sadowski T (2014) Simulations of post-impact skin/core debond growth in sandwich plates under impulsive loading. Journal of Applied Nonlinear Dynamics 3(4):369 – 379

Burlayenko VN, Sadowski T (2018) Linear and nonlinear dynamic analyses of sandwich panels with face sheet-to-core debonding. Shock and Vibration 2018(ID 5715863)

Burlayenko VN, Sadowski T, Pietras D (2018) A numerical analysis of near tip fields in a bending moment-loaded double cantilever sandwich beam fracture specimen. Bulletin of NTU "KhPI" 3(1279):9 – 14

Burlayenko VN, Altenbach H, Sadowski T (2019a) Dynamic fracture analysis of sandwich composites with face sheet/core debond by the finite element method. In: Altenbach H, Belyaev A, Eremeyev V, Krivtsov A, Porubov A (eds) Dynamical Processes in Generalized Continua and Structures, Advanced Structured Materials, vol 103, Springer, Singapore, pp 163–194

Burlayenko VN, Pietras D, Sadowski T (2019b) Influence of geometry, elasticity properties and boundary conditions on the Mode I purity in sandwich composites. Composite Structures 223, 110942

Burlayenko VN, Sadowski T, Pietras D (2019c) Influence of dynamic loading on fracture behaviour of DCB sandwich specimen. ITM Web Conf 29, 02003 DOI 10.1051/itmconf/20192902003

Cantwell W, Davies P (1996) A study of skin-core adhesion in glass fibre reinforced sandwich materials. Applied Composite Materials 3(6):407 – 420

Cantwell WJ, Scudamore R, Ratcliffe J, Davies P (1999) Interfacial fracture in sandwich laminates. Composites Science and Technology 59(14):2079 – 2085

Carlsson LA, Sendlein LS, Merry SL (1991) Characterization of face sheet/core shear fracture of composite sandwich beams. Journal of Composite Materials 25(1):101 – 116

Chatterjee VA, Verma SK, Bhattacharjee D, Biswas I, Neogi S (2019) Enhancement of energy absorption by incorporation of shear thickening fluids in 3d-mat sandwich composite panels upon ballistic impact. Composite Structures 225:111,148

Crews JH, Shivakumar KN, Raju IS (1991) Strain energy release rate distributions for double cantilever beam specimens. AIAA Journal 29(10):1686 – 1691

Davidson BD, Hu H, Schapery RA (1995) An analytical crack-tip element for layered elastic structures. Trans ASME Journal of Applied Mechanics 62(2):295 – 305

Davis BR, Wawrzynek PA, Ingraffea AR (2014) 3-D simulation of arbitrary crack growth using an energy-based formulation – Part I: Planar growth. Engineering Fracture Mechanics 115:204 – 220

Dillard DA, Singh HK, Pohlit DJ, Starbuck JM (2009) Observations of decreased fracture toughness for mixed mode fracture testing of adhesively bonded joints. Journal of Adhesion Science and Technology 23(10 - 11):1515 – 1530

Farhana N, Majid MA, Paulraj M, Ahmadhilmi E, Fakhzan M, Gibson A (2016) A novel vibration based non-destructive testing for predicting glass fibre/matrix volume fraction in composites using a neural network model. Composite Structures 144:96 – 107

Fichter WB (1983) The stress intensity factor for the double cantilever beam. International Journal of Fracture 22:133 – 143

Georgiadis HG, Papadopoulos GA (1990) Elastostatics of the orthotropic double-cantilever-beam fracture specimen. Zeitschrift für angewandte Mathematik und Physik ZAMP 41(6):889 – 899

Harne RL, Blanc C, Remillieux MC, Burdisso RA (2012) Structural-acoustic aspects in the modeling of sandwich structures and computation of equivalent elasticity parameters. Thin-Walled Structures 56:1 – 8

Hernández-Pérez A, Avilés F, Carlsson L (2013) Evaluation of the plate twist test to characterize mode iii fracture of sandwich panels with a face/core interface crack. Engineering Fracture Mechanics 104:41 – 55

Hutchinson JW, Suo Z (1991) Mixed mode cracking in layered materials. In: Hutchinson JW, Wu TY (eds) Advances in Applied Mechanics, vol 29, Elsevier, pp 63 – 191

Idriss M, Mahi AE (2017) Effects of debonding length on the fatigue and vibration behaviour of sandwich composite. Journal of Composite Materials 51(13):1839 – 1847

Kardomateas GA, Berggreen C, Carlsson LA (2013) Energy-release rate and mode mixity of face/core debonds in sandwich beams. AIAA Journal 51(4):885–892

Kiss B, Szekrényes A (2019) Fracture and mode mixity analysis of shear deformable composite beams. Archive of Applied Mechanics 89(12):2485 – 2506

Kuang-Chong W (1991) Explicit crack-tip fields of an extending interface crack in an anisotropic bimaterial. International Journal of Solids and Structures 27(4):455 – 466

Kuna M (2013) Finite Elements in Fracture Mechanics: Theory - Numerics - Applications. Springer, Dordrecht

Li S, Wang J, Thouless MD (2004) The effects of shear on delamination in layered materials. Journal of the Mechanics and Physics of Solids 52(1):193 – 214

Li X, Carlsson LA (1999) The tilted sandwich debond (tsd) specimen for face/core interface fracture characterization. Journal of Sandwich Structures & Materials 1(1):60–75

Lu L, Song H, Yuan W, Huang C (2017) Baseline-free damage identification of metallic sandwich panels with truss core based on vibration characteristics. Structural Health Monitoring 16(1):24 – 38

Massabò R, Campi F (2014) Assessment and correction of theories for multilayered plates with imperfect interfaces. Meccanica 50:1045–1071

Matos PPL, McMeeking RM, Charalambides PG, Drory MD (1989) A method for calculating stress intensities in bimaterial fracture. International Journal of Fracture 40:235 – 254

Mouritz AP (2017) Progress toward explosive blast-resistant naval composites. In: Mouritz AP, Rajapakse YD (eds) Explosion Blast Response of Composites, Woodhead Publishing, pp 375 – 408

Mustapha S, Ye L (2013) 10 - non-destructive evaluation (nde) of composites: assessing debonding in sandwich panels using guided waves. In: Karbhari VM (ed) Non-Destructive Evaluation (NDE) of Polymer Matrix Composites, Woodhead Publishing Series in Composites Science and Engineering, Woodhead Publishing, pp 238 – 278

Odessa I, Frostig Y, Rabinovitch O (2018) Modeling of interfacial debonding propagation in sandwich panels. International Journal of Solids and Structures 148-149:67 – 78

Pölöskei T, Szekrényes A (2017) Quasi-periodic excitation in a delaminated composite beam. Composite Structures 159:677 – 688

Prasad S, Carlsson LA (1994) Debonding and crack kinking in foam core sandwich beams — I. Analysis of fracture specimens. Engineering Fracture Mechanics 47(6):813 – 824

Qu Y, Meng G (2017) Nonlinear vibro-acoustic analysis of composite sandwich plates with skin–core debondings. AIAA Journal 55(5):1723 – 1733

Quispitupa A, Berggreen C, Carlsson LA (2009) On the analysis of a mixed mode bending sandwich specimen for debond fracture characterization. Engineering Fracture Mechanics 76(4):594 – 613

Ratcliffe JG, Reeder JR (2011) Sizing a single cantilever beam specimen for characterizing facesheet–core debonding in sandwich structure. Journal of Composite Materials 45(25):2669 – 2684

Rice JR (1988) Elastic fracture mechanics concepts for interfacial cracks. Trans ASME Journal of Applied Mechanics 55(1):98 – 103

Rinker M, John M, Zahlen PC, Schäuble R (2011) Face sheet debonding in CFRP/PMI sandwich structures under quasi-static and fatigue loading considering residual thermal stress. Engineering Fracture Mechanics 78(17):2835 – 2847

Rodríguez-González J, May-Pat A, Avilés F (2014) A beam specimen to measure the face/core fracture toughness of sandwich materials under a tearing loading mode. International Journal of Mechanical Sciences 79:84 – 94

Ryoji Y, Sang-Bong C (1989) Efficient boundary element analysis of stress intensity factors for interface cracks in dissimilar materials. Engineering Fracture Mechanics 34(1):179 – 188

Samborski S (2018) Prediction of delamination front's advancement direction in the CFRP laminates with mechanical couplings subjected to different fracture toughness tests. Composite Structures 202:643 – 650

Saseendran V, Carlsson LA, Berggreen C (2018) Shear and foundation effects on crack root rotation and mode-mixity in moment- and force-loaded single cantilever beam sandwich specimen. Journal of Composite Materials 52(18):2537 – 2547

Seguel F, Meruane V (2018) Damage assessment in a sandwich panel based on full-field vibration measurements. Journal of Sound and Vibration 417:1 – 18

Shih CF, Asaro RJ (1988) Elastic-plastic analysis of cracks on bimaterial interfaces: Part I — Small scale yielding. Trans ASME Journal of Applied Mechanics 55(2):299 – 316

Shivakumar KN, Smith SA (2004) In situ fracture toughness testing of core materials in sandwich panels. Journal of Composite Materials 38(8):655 –668

Smelser RE (1979) Evaluation of stress intensity factors for bi-materials bodies using numerical crack flank displacement data. International Journal of Fracture 15:135 – 315

Sorensen B, Jorgensen K, Jacobsen T, Ostergaard R (2006) DCB-specimen with uneven bending moments. International Journal of Fracture 141:163–176

Suo Z, Hill R (1990) Singularities, interfaces and cracks in dissimilar anisotropic media. Proceedings of the Royal Society of London A Mathematical and Physical Sciences 427(1873):331 – 358

Suo Z, Hutchinson JW (1990) Interface crack between two elastic layers. International Journal of Fracture 43:1 – 18

Thouless MD (2018) Shear forces, root rotations, phase angles and delamination of layered materials. Engineering Fracture Mechanics 191:153 – 167

Triantafillou TC, Gibson LJ (1987) Failure mode maps for foam core sandwich beams. Materials Science and Engineering 95:37 – 53

Valvo PS, Sorensen BF, Toftegaard HL (2015) Modelling the double cantilever beam test with bending moments by using bilinear discontinuous cohesive laws. In: Proceedings of the 20th International Conference on Composite Materials Copenhagen, 19-24 July 2015

Wang J, Qiao P (2004) On the energy release rate and mode mix of delaminated shear deformable composite plates. International Journal of Solids and Structures 41(9):2757 – 2779

Wang TC, Shih CF, Zhigang S (1992) Crack extension and kinking in laminates and bicrystals. International Journal of Solids and Structures 29(3):327 – 344

Williams JG (1988) On the calculation of energy release rate for cracked laminates. International Journal of Fracture 36:101 – 119

Williams TO, Addessio FL (1997) A general theory for laminated plates with delaminations. International Journal of Solids and Structures 34(16):2003 – 2024

Willis JR (1971) Fracture mechanics of interfacial cracks. Journal of the Mechanics and Physics of Solids 19(6):353 – 368

Xie S, Liang X, Zhou H (2016) Design and analysis of a composite energy-absorbing structure for use on railway vehicles. Proceedings of the Institution of Mechanical Engineers, Part F: Journal of Rail and Rapid Transit 230(3):825 – 839